

# Nanoscale

Accepted Manuscript



This is an *Accepted Manuscript*, which has been through the Royal Society of Chemistry peer review process and has been accepted for publication.

*Accepted Manuscripts* are published online shortly after acceptance, before technical editing, formatting and proof reading. Using this free service, authors can make their results available to the community, in citable form, before we publish the edited article. We will replace this *Accepted Manuscript* with the edited and formatted *Advance Article* as soon as it is available.

You can find more information about *Accepted Manuscripts* in the [Information for Authors](#).

Please note that technical editing may introduce minor changes to the text and/or graphics, which may alter content. The journal's standard [Terms & Conditions](#) and the [Ethical guidelines](#) still apply. In no event shall the Royal Society of Chemistry be held responsible for any errors or omissions in this *Accepted Manuscript* or any consequences arising from the use of any information it contains.

# 1 Functionalized Iron Oxide Nanoparticles for Controlling the Movement of 2 Immune Cells

3 **Ethan E White<sup>a, c, e</sup>, Alex Pai<sup>d, e</sup>, Yiming Weng<sup>a, e</sup>, Anil K. Suresh<sup>a, e</sup>, Desiree Van Haute<sup>a, c</sup>,**  
4 **Torkom Pailevanian<sup>d</sup>, Darya Alizadeh<sup>a, b</sup>, Ali Hajimiri<sup>d, \*</sup>, Behnam Badie<sup>b, \*</sup> and Jacob M.**  
5 **Berlin<sup>a, \*</sup>**

6 <sup>a</sup> Department of Molecular Medicine, <sup>b</sup> Division of Neurosurgery, Department of Surgery,  
7 Beckman Research Institute, <sup>c</sup> Irell & Manella Graduate School of Biological Sciences at City of  
8 Hope, 1500 East Duarte Road, Duarte, CA, 91010, United States.

9 <sup>d</sup> Department of Electrical Engineering, California Institute of Technology, 1200 E. California  
10 Blvd., Pasadena, CA 91125, United States.

11 <sup>e</sup> These authors contribute equally.

12 \* Drs. Hajimiri, Badie, and Berlin, served as co-PI's for these studies. Contact info:

13 E-mail: jberlin@coh.org. Tel.: +1 626 256 4673

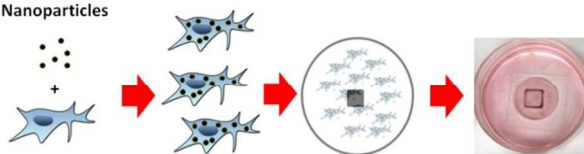
14 E-mail: bbadie@coh.org. Tel.: +1 626 256 4673.

15 E-mail: hajimiri@caltech.edu. Tel.: +1 626 395 2312.

16

## 17 Table of Contents

Coated Iron Oxide  
Nanoparticles



18 Microglia

Magnet Under Dish

19 Coating super paramagnetic iron oxide nanoparticles with an immunostimulant, CpG  
20 oligodeoxynucleotides, dramatically increases their uptake by microglia cells. Once loaded with the  
21 nanoparticles, the microglia cells can be manipulated with magnets.

22

## 23 Abstract

24 Immunotherapy is currently being investigated for the treatment of many diseases, including  
25 cancer. The ability to control the location of immune cells during or following activation would  
26 represent a powerful new technique for this field. Targeted magnetic delivery is emerging as a  
27 technique for controlling cell movement and localization. Here we show that this technique can  
28 be extended to microglia, the primary phagocytic immune cells in the central nervous system.  
29 The magnetized microglia were generated by loading the cells with iron oxide nanoparticles  
30 functionalized with CpG oligonucleotides, serving as a proof of principle that nanoparticles can  
31 be used to both deliver an immunostimulatory cargo to cells and to control the movement of the  
32 cells. The nanoparticle-oligonucleotide conjugates are efficiently internalized, non-toxic, and  
33 immunostimulatory. We demonstrate that the *in vitro* migration of the adherent, loaded  
34 microglia can be controlled by an external magnetic field and that magnetically-induced  
35 migration is non-cytotoxic. In order to capture video of this magnetically-induced migration of

36 loaded cells, a novel 3D-printed “cell box” was designed to facilitate our imaging application.  
37 Analysis of cell movement velocities clearly demonstrate increased cell velocities toward the  
38 magnet. These studies represent the initial step towards our final goal of using nanoparticles to  
39 both activate immune cells and to control their trafficking within the diseased brain.  
40

## 41 **1. Introduction**

42 Immunotherapy is an attractive treatment strategy for many diseases, including cancer.<sup>1</sup>  
43 Generally, this strategy involves stimulating the immune system such that it recognizes the  
44 diseased cells as foreign and eliminates them. A wide variety of agents, ranging from antibodies,  
45 to engineered immune cells, to potent adjuvants have been used to stimulate the immune system.  
46 Immunotherapy would be greatly enhanced as a treatment strategy if the location of the immune  
47 cells both during and after stimulation could be controlled. For the case of cancer  
48 immunotherapy, it could be of great benefit to direct activated immune cells to the tumor in order  
49 to promote antigen recognition specifically for cancer cells. Furthermore, the immune response  
50 could be enhanced by maintaining a population of activated immune cells at the primary tumor  
51 site and/or improving the trafficking of activated immune cells to distant foci of disease.

52 We have been pursuing the use of oligodeoxynucleotides that contain an unmethylated  
53 CpG motif (CpG) as immune stimulants for the treatment of glioblastoma. CpG is known to be  
54 immunostimulatory by activating toll like receptor-9 (TLR9) which is expressed by normal and  
55 glioma-associated human microglia and macrophages.<sup>2-5</sup> Activation of TLRs enhances the  
56 uptake of microorganisms by phagocytic cells, promotes secretion of Th1 cytokines, and  
57 mediates leukocyte recruitment to infected tissues. TLR9 is not found on the cell surface, but is  
58 initially located in the endoplasmic reticulum (ER) and is then found colocalized with CpGs in  
59 the lysosomes following stimulation.<sup>6</sup> Therefore, because CpG-induced immune stimulation is  
60 dependent upon TLR9 interacting with CpG inside the endosomal compartment, using a platform  
61 that achieves endosomal delivery of CpG may be an attractive strategy for enhancing CpG  
62 efficacy.<sup>7</sup>

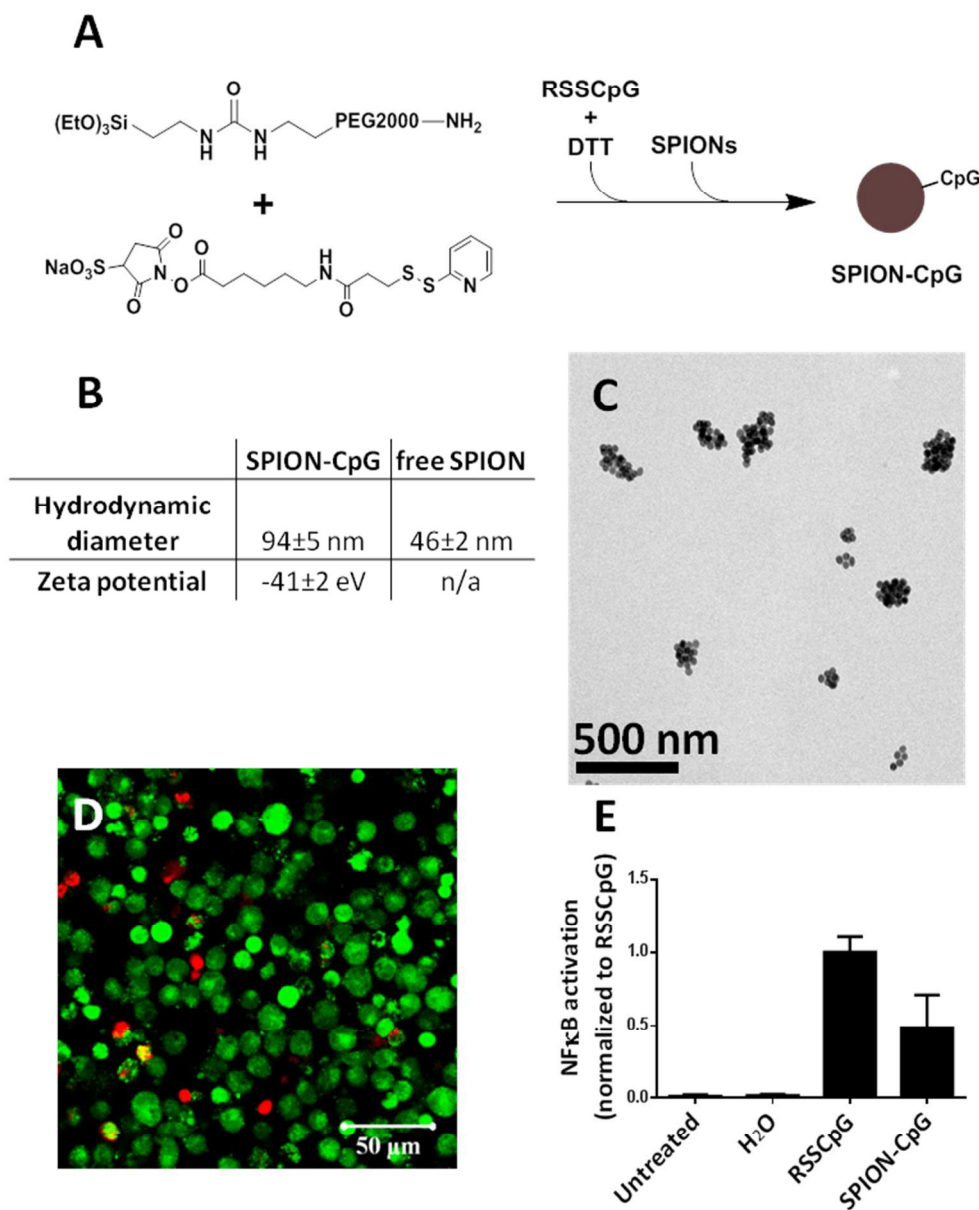
63 Nanoparticles are appealing delivery platforms for CpG because, in general,  
64 nanoparticles are rapidly endocytosed by phagocytic immune cells.<sup>8</sup> Various nanoparticles have  
65 been investigated as potential candidates for the delivery of CpGs, including liposomes,<sup>9</sup> self-  
66 assembling DNA nanoparticles,<sup>10</sup> poly(lactic-co-glycolic acid) nanoparticles<sup>11</sup> and gold  
67 nanoparticles.<sup>12</sup> For the treatment of brain cancers, we recently reported that the use of single-  
68 walled carbon nanotubes as delivery vehicles for CpG dramatically increased the efficacy of the  
69 CpG, such that a *single* intracranial injection of the nanotube-CpG construct cured 60% of  
70 glioma-bearing mice.<sup>13, 14</sup> Moreover, when mice that were cured by treatment with the nanotube-  
71 CpG construct were rechallenged with a subcutaneous injection of GL261 glioma cells, every  
72 mouse rejected the cancer cells, demonstrating a successful induction of systemic immunity.

73 This nanotube-CpG construct is readily taken up by macrophages, microglia, NK cells  
74 and dendritic cells.<sup>13</sup> We hypothesized that using super paramagnetic iron oxide nanoparticles  
75 (SPIONs) as the delivery platform for the CpG would enable magnetic control of immune cells  
76 that endocytosed the particles. SPIONs respond to magnetic fields and allow for the controlled  
77 delivery of conjugated chemotherapeutics.<sup>15</sup> This technique may even allow for targeted  
78 delivery deep within the body.<sup>16, 17</sup> Magnetic targeting of drug delivery has been applied to brain  
79 tumors.<sup>18</sup> Recently, magnetic targeting has been extended to cells by labeling desired cell  
80 populations with SPIONs and other magnetic particles. One focus of this work has been  
81 attracting loaded cells to magnetized implanted devices, such as stents.<sup>19, 20</sup> Another primary  
82 application has been targeting loaded stem cells for regenerative medicine.<sup>21-24</sup> A limited number  
83 of publications have also described magnetic control of loaded immune cells.<sup>25</sup> Clinically, we  
84 envision that a SPION-based immunotherapy could be injected intracranially, internalized by

85 local immune cells, and then enable the magnetically-controlled migration of these activated  
86 immune cells for the treatment of multifocal disease or deep brain tumors.

87 Here we demonstrate that SPION-CpG conjugates are efficiently internalized by  
88 microglia which allows for magnetic control of the loaded cells. The synthesis and  
89 characterization of the SPION-CpG conjugates is described. Furthermore, the SPION-CpG  
90 conjugates are shown to be non-toxic and immunostimulatory.

91



92  
 93 **Figure 1:** Synthesis and characterization of the SPION-CpG conjugates. (A) Schematic  
 94 illustration of the synthesis of SPION-CpG conjugates. (B) Hydrodynamic diameter and zeta  
 95 potential of SPION-CpG conjugates. (C) Transmission electron microscopy image of the  
 96 SPION-CpG conjugates. (D) LIVE/DEAD stain of N9 cells treated with 0.5 mg/mL for 12 h.  
 97 Red = ethidium homodimer (dead), green = calcein AM (live). (E) NFκB activation of RAW-

98 Blue™ mouse macrophage reporter cells treated with 0.1 mg/mL SPION-CpG (n=2, 6 replicates  
99 each). The average of the normalized data from two assays is shown.

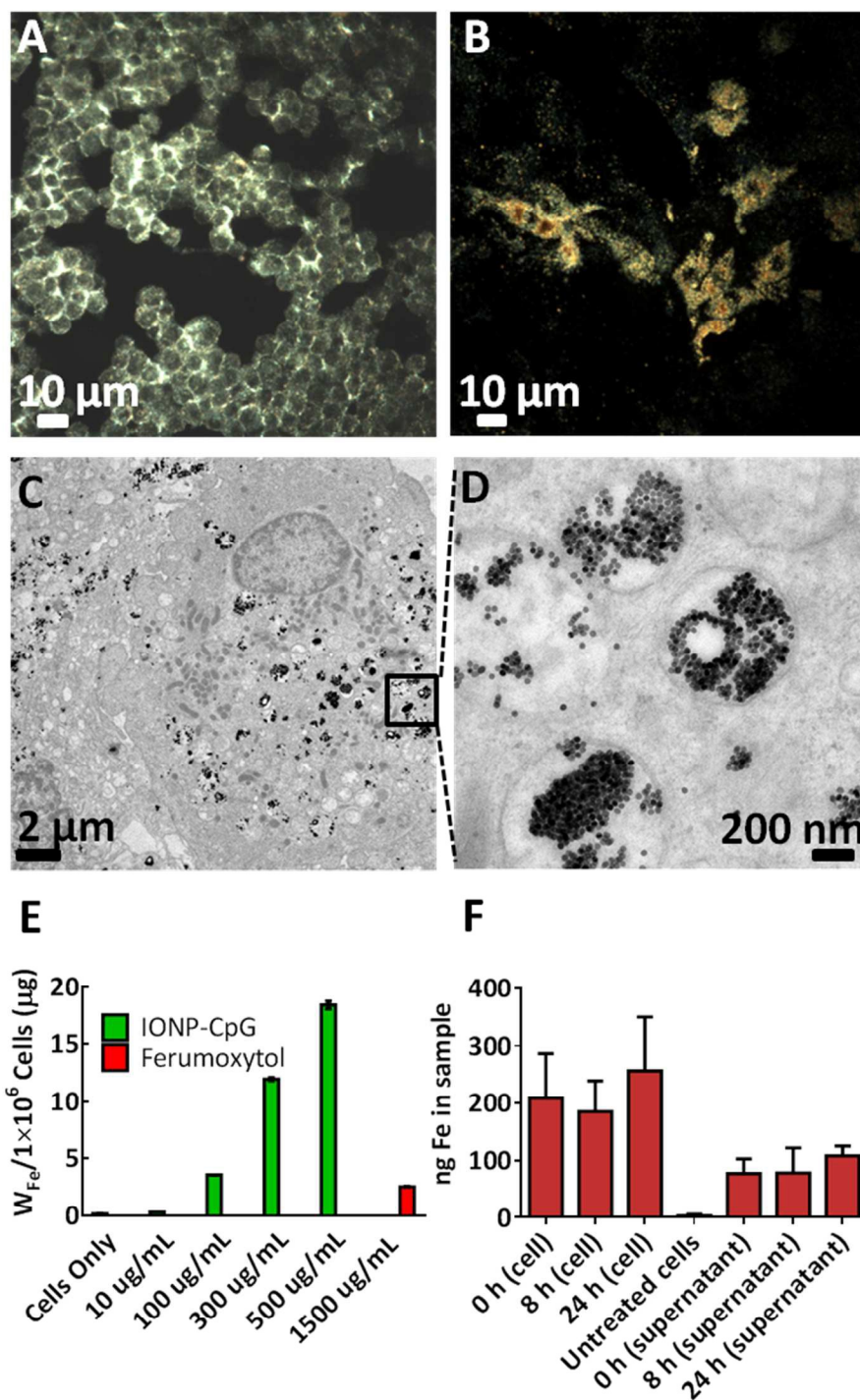
100

## 101 2. Results and discussion

102 The long-term goal of this research is to generate an iron-oxide-based cancer  
103 immunotherapy that enables magnetically-guided, modular localization of activated immune  
104 cells *in vivo*. The objective of this manuscript is to provide proof-of-principle evidence that  
105 adherent, microglia-like immune cells can be loaded with immunostimulatory particles and  
106 moved by magnetic fields *in vitro*. To perform the *in vitro* magnetic field influenced cell  
107 movement studies, SPION-CpG conjugates (Fig 1A) were prepared from 30 nm SPIONs (Fig  
108 S1A). The synthetic protocol was intended to produce CpG conjugated to PEG with a terminal  
109 silyl ether for conjugation to the SPIONs, but Mass Spectrometry (MS) analysis (Fig S1C)  
110 indicated that the reduction of RSSCpG was inefficient and thus the majority of material used to  
111 coat the SPIONs was likely RSSCpG. Nonetheless, it was clear that a functional coating was  
112 achieved as demonstrated by the change in aqueous stability of the SPIONs. The as-received  
113 SPIONs were coated with oleic acid and thus not miscible with water, but, following sonication  
114 with the CpG-containing material, the SPIONs entered the aqueous phase. Furthermore, zeta  
115 potential measurements showed the resulting SPION-CpG particles to be negatively charged,  
116 consistent with an oligonucleotide coating (Fig 1B). Dynamic light scattering measurements  
117 indicated that the SPION-CpG conjugates have a hydrodynamic diameter of  $94\pm 5$  nm, as  
118 compared to  $46\pm 2$  nm for the free SPIONs (Fig 1B). This is likely the result of small aggregates  
119 forming following the coating, as revealed by transmission electron microscopy (TEM, Fig 1C).

120 Cell assays indicated that SPION-CpG was both non-cytotoxic (Fig 1D) and  
121 immunostimulatory (Fig 1E). The LIVE/DEAD assay was used to evaluate cell viability of N9  
122 mouse microglia cells after 12 h of loading at SPION-CpG concentrations up to 0.5 mg/mL. As  
123 shown in Fig 1D and Fig S1D, the treated cells exhibited an equivalent level of viability as  
124 untreated control cells. In order to evaluate the immunostimulatory potential of SPION-CpG, an  
125 NFκB reporter cell line was used. Because NFκB activity is increased in response to TLR9  
126 activation by CpG, immune stimulation by SPION-CpG was expected to cause an increase in  
127 NFκB signal within this reporter system. Indeed, SPION-CpG treatment induced an increase in  
128 NFκB activity when compared to untreated cells (Fig 1E). However, the NFκB activity of  
129 SPION-CpG was less than an equivalent amount of free CpG (RSSCpG). This reduction in  
130 activity has several possible causes. It is possible that some CpG was lost during the SPION-  
131 CpG synthesis process, thus resulting in lower NFκB activity after uptake by reporter cells. It is  
132 also possible that the immunostimulatory activity of CpG was partially inhibited by conjugation  
133 to SPIONs. Phosphate groups are well-known for their ability to bind the surface of iron oxide.<sup>26</sup>  
134 <sup>27</sup> Therefore it is likely that the phosphorothioate backbone of the CpG oligonucleotide interacted  
135 with the surface of the SPIONs, interfering with CpG release or its binding to TLR9.<sup>28</sup> Future  
136 work will focus on investigating the mechanism of this phenomenon and further enhancing the  
137 immunostimulatory activity of SPION-CpG.

138



139

140 **Figure 2:** SPION-CpG is internalized in N9 cells. Dark-field images of (A) microglia cells alone

141 and (B) cells loaded with SPION-CpG conjugates [0.5 mg/mL]. (C-D) TEM images of loaded

142 cells. ICP-MS analysis of (E) cells treated with increasing concentrations of SPION-CpG

143 conjugates and Ferumoxytol. (F) Cell and supernatant fractions at various time points after  
144 loading (n=2 with treatments performed in triplicate, average of two experiments is shown).  
145 Error bars represent standard deviations of iron content in replicate wells.

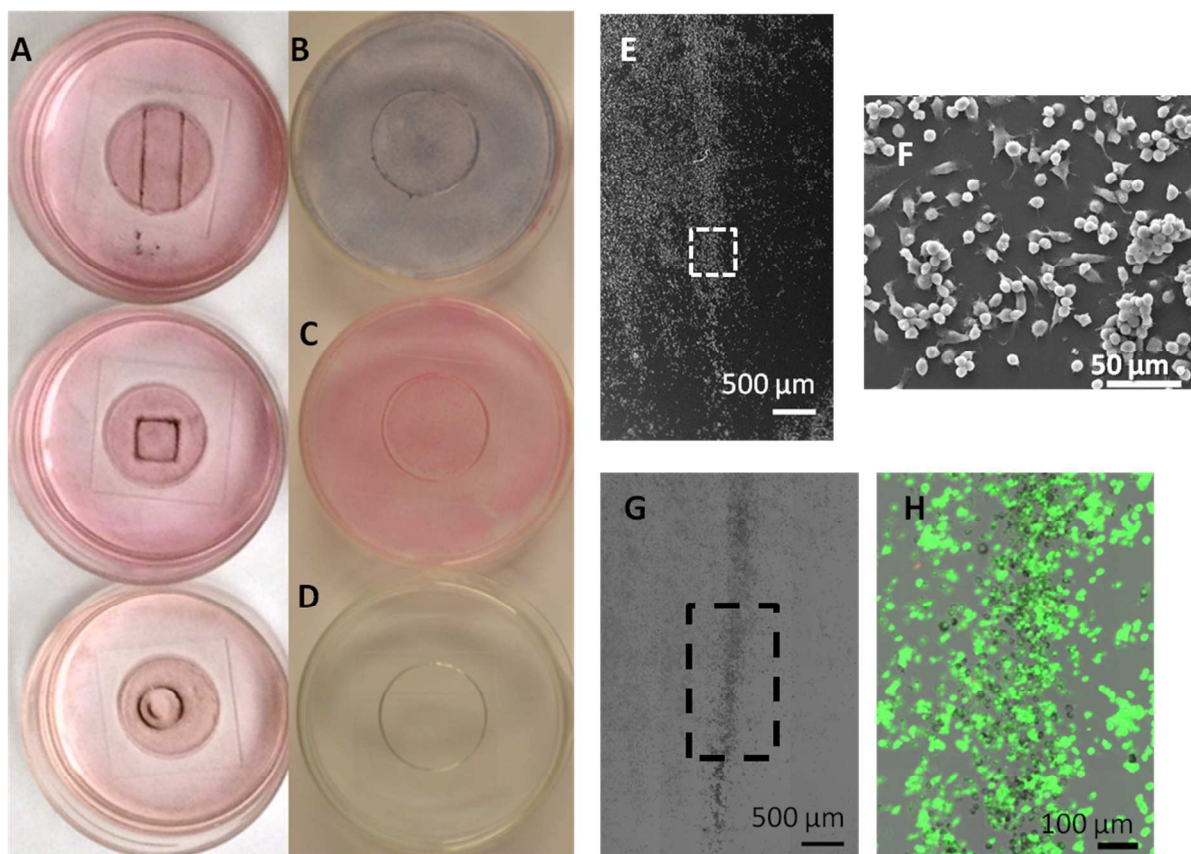
146

147       Next, inductively coupled plasma mass spectrometry (ICP-MS) was used to quantify the  
148 cellular uptake of the SPION-CpG by N9 microglia. Briefly, cells were treated with increasing  
149 concentrations (0, 0.01, 0.1, 0.3 and 0.5 mg/mL) of SPION-CpG conjugates for 12 h, washed  
150 thoroughly, digested with nitric acid and analyzed using ICP-MS. A dose-dependent increase in  
151 iron content above the normal background level in control cells was observed (Fig 2E). For  
152 comparison, cells were also treated with the commercially available Ferumoxytol iron oxide  
153 nanoparticles (sold under the name Feraheme®), which are approved for human use by the US  
154 Food and Drug Administration. Ferumoxytol particles are similar in size to the SPIONs used in  
155 this study, with an iron core diameter of 17-30 nm.<sup>29</sup> However, even when cells were exposed to  
156 a 3× higher concentration of Ferumoxytol as compared to SPION-CpG, very little uptake of the  
157 Ferumoxytol particles was observed. While there are a number of differences between our  
158 SPION-CpG and Ferumoxytol, we speculate that this increased loading of SPION-CpG was due  
159 to the oligonucleotide coating. It has previously been shown that oligonucleotide coatings lead to  
160 enhanced cell uptake mediated by scavenger receptors.<sup>30, 31</sup> Independent of the mechanism  
161 responsible, the enhanced uptake for our SPION-CpG made this material appealing for use in the  
162 magnetic control of microglia.

163       Further, dark-field microscopy imaging was performed to show the uptake and  
164 distribution of the particles over a relatively large area. N9 cells treated with SPION-CpG  
165 conjugates at a concentration of 0.5 mg/mL were assessed using a dark-field microscope.

166 Untreated control cells showed no uptake (Fig 2A), whereas cells treated with SPION-CpG  
167 conjugates showed profound uptake of the SPIONs (Fig 2B). TEM imaging was also performed  
168 to gather information on the intracellular distribution of the SPION-CpG conjugates. At low  
169 magnification, TEM imaging performed across various regions of the grid revealed strong uptake  
170 of the SPION-CpG conjugates, in agreement with dark-field microscopy. Higher magnification  
171 TEM imaging showed dense aggregates of particles that were predominantly located in  
172 intracellular vesicles (Fig 2C-D). Some particles were observed in the cytoplasm as well, and no  
173 particles were found in the nucleus. Similarly, no uptake was observed in the untreated control  
174 cells (Fig S2A-B).

175         After verifying that SPION-CpG was internalized by N9 cells, the exocytosis of these  
176 particles was then investigated. This has important implications in experiments involving  
177 magnetically-induced movement. As a cell exocytoses SPIONs, its responsiveness to magnetic  
178 fields will decrease as a function of the amount of residual intracellular iron. Thus the rate of  
179 exocytosis affects the time period over which the cells can be moved *in vitro*. In order to track  
180 the rate of exocytosis, N9 cells were loaded and the iron content of both the cells and the cell  
181 media was measured at 0, 8, and 24 h after loading. Over a 24 h period, there was no detectable  
182 increase in the iron content of the cell media nor was there a detectable decrease in the iron  
183 content of the cell fraction (Fig 2F). Therefore, we concluded that exocytosis of SPION-CpG  
184 was negligible in N9 cells over 24 h. The background iron level in the media at 0 h was  
185 presumably residual free SPION-CpG which was not removed when the loaded cells were  
186 washed with PBS two times. Longer time points were not investigated because 24 h proved  
187 sufficient to demonstrate robust *in vitro* movement.



188  
189 **Figure 3:** Magnetically induced movement of the cells loaded with SPION-CpG conjugates. (A)  
190 Color images of loaded cells after exposure to magnets of different shapes for 20 h. The  
191 concentration of SPION-CpG used for loading was 0.1 mg/mL. (B-D) are the various controls  
192 used for the magnetic movement experiments; (B) loaded cells not exposed to the magnet, (C)  
193 unloaded cells exposed to the magnet, and (D) SPION-CpG only without cells. (E-F) SEM  
194 images of cells after movement. (G-H) Brightfield and fluorescent images of LIVE/DEAD-  
195 stained cells after movement.

196  
197 As a simple test to evaluate if SPION-CpG-loaded microglia could be controlled with an  
198 external magnetic field, three different shaped magnets were placed underneath glass bottom  
199 culture dishes containing adherent N9 cells loaded with SPION-CpG. After 20 h, the media was

200 aspirated, the plates were stained with Prussian blue, and photographs were taken to demonstrate  
201 the shape-dependent localization of the loaded cells (Fig 3A). Additionally, this magnetically  
202 controlled cell movement was correlated with the dose of SPION-CpG given to the cells, with  
203 higher loadings leading to more pronounced accumulation at the magnet (Fig S3A-C). As  
204 controls, we also imaged SPION-CpG particles only with magnet exposure, untreated cells with  
205 magnetic exposure and cells loaded with SPION-CpG that were not exposed to any magnets. The  
206 SPION-CpG only control shows almost no adherence of the particles, such that following  
207 staining and washing, very little material remained in the dish (Fig 3D). Neither “empty” cells  
208 that were exposed to the magnet nor loaded cells not exposed to the magnet migrated *in vitro*,  
209 confirming that the shape-dependent localization of the loaded cells was magnetically controlled  
210 (Fig 3B-C). In order to more closely monitor the magnetically induced migration of the cells,  
211 higher magnification images were recorded for loaded cells after 0, 2, 4, and 20 h of magnet  
212 exposure (Fig S4M-P). Accumulation of the loaded cells at the edge of the magnet where the  
213 magnetic field gradient was largest was observed by 4 h and increased until 20 h. Collectively,  
214 these controls demonstrate that the accumulation at the edge of the magnet was due to SPION-  
215 loaded cells moving in response to the magnetic field.

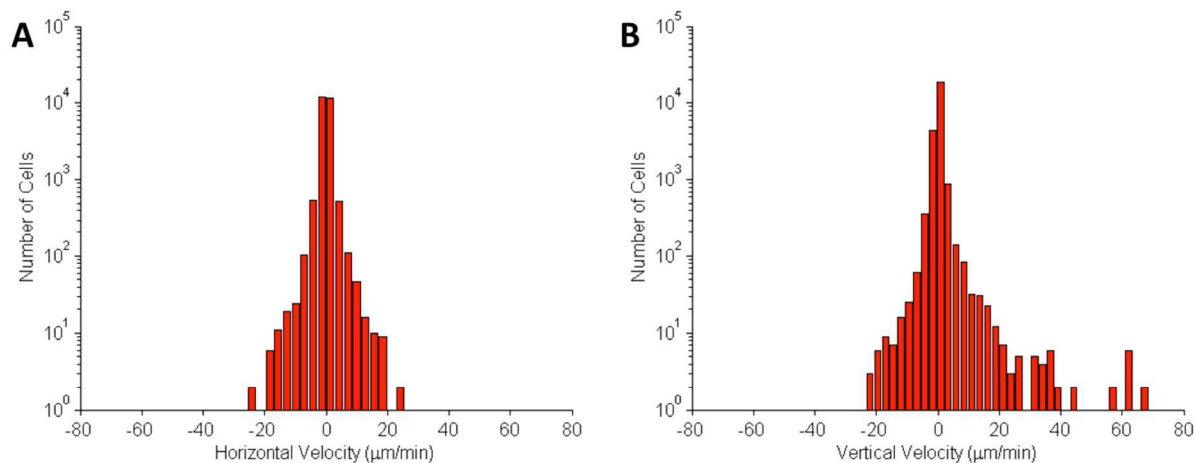
216 In order to verify that magnetically-induced movement was nontoxic, the migrated cells  
217 were examined for changes in viability and cell morphology. Because the migrated cells  
218 comprise only a small percentage of the total cell population of the dish, assays that analyze the  
219 bulk cell population would not be able to detect changes in the migrated cell population due to a  
220 high background signal from the non-migrated cells. Furthermore, there is no good way to  
221 separate the migrated and non-migrated cell populations prior to analysis. Therefore, analysis of  
222 the migrated population was performed using imaging-based techniques. Imaging-based

223 techniques allow the spatial information from the cells to be preserved during the analysis,  
224 enabling quick identification of migrated and non-migrated populations.

225 Viability and cell morphology were examined via the LIVE/DEAD assay and SEM,  
226 respectively. After loaded cells were exposed to the magnet for 20 h and clear migration was  
227 observed, the cells in the dish were stained with calcein AM and ethidium homodimer, fixed, and  
228 then fluorescently imaged to assess viability. After fluorescent imaging, the same region of cells  
229 was imaged by SEM. No decrease in cell viability was detected for migrated cells nor were any  
230 gross abnormalities in cell morphology observed (Fig 3E-H, S3D-G).

231 The movement of magnetized cells is primarily determined by the external magnetic field  
232 profile and strength, the hydrodynamic properties of the cell in its environment, and the  
233 effectiveness of SPION uptake by the cells. An important evaluation of cell motility is the  
234 quantification of movement velocity. Therefore, in order to analyze the movement velocity of  
235 cells, an innovative imaging, incubation, and magnetic manipulation apparatus was designed to  
236 track magnetized cells in magnetic fields (Fig S4Q). The apparatus consists of a custom “cell  
237 box” fitted onto a standard sized petri dish. N9 cells were plated onto the coverslip portion of  
238 the cell box and then loaded with SPION-CpG. After cell loading, the entire box assembly was  
239 then inverted into a petri dish containing culture medium. For time-lapse imaging, the cell box  
240 and petri dish were placed onto the stage of an inverted microscope equipped with incubation  
241 capabilities. A ceramic permanent magnet was then placed on the opposite side of the coverslip  
242 to which the cells were attached.

243



244 **Figure 4:** Histograms of (A) horizontal and (B) vertical cell velocities in motility experiment.  
 245

246 Magnetized cells were imaged over a period of 12 h under the exposure of a magnetic field. The  
 247 external magnet was placed in the positive vertical position to the cells. Velocities were  
 248 calculated by extracting the change in cell position from one frame to the next. The average  
 249 velocity was  $0.2 \pm 3.72 \mu\text{m}/\text{min}$  and the vertical direction and  $0.03 \pm 1.69 \mu\text{m}/\text{min}$  in the horizontal  
 250 direction.

251  
 252 During magnet exposure, the cells were imaged at 2 frames/min for a period of 20 h.  
 253 Cell positions were extracted using an image processing algorithm.<sup>32</sup> The distribution of cell  
 254 velocities in the vertical direction (toward the magnet) and horizontal direction is shown in Fig  
 255 4A-B. The histograms in Fig 4A-B show that the cell movement in the horizontal direction was  
 256 symmetrical, while cell movement in the vertical direction was skewed toward the externally-  
 257 applied magnetic field. In some cases cells migrated toward the magnet at velocities exceeding  
 258  $30 \mu\text{m}/\text{min}$ .

259

260

### 261 3. Experimental

262 Ultrasonication was performed using a QSONICA Sonicator Q700 (QSONICA, Newtown, CT,  
263 USA) equipped with a cup horn cooled with running water from the sink. Super paramagnetic  
264 iron oxide nanoparticles (30 nm, catalogue #SOR-30) were purchased from Ocean Nanotech,  
265 Springdale, AR, USA. Silane-PEG-NH<sub>2</sub> (MW = 2000, Catalogue #PG2-AMSL-2k) was  
266 purchased from NANOCS. Dithiotheritol (DTT) was purchased from VWR. Fully  
267 phosphorothioated CpG oligonucleotides bearing a terminal dithiol (5-HO-C<sub>6</sub>-SS-C<sub>6</sub>-  
268 T\*A\*A\*A\*C\*G\*T\*T\*A\*T\*A\*A\*C\*G\*T\*T\*A\*T\*G\*A\*C\*G\*T\*C\*A\*T\*-3) (RSS-CpG) was  
269 provided by the DNA core facility at Beckman Research Institute at City of Hope.  
270 Sulfosuccinimidyl 6-(3'-[2-pyridyldithio]-propionamido)hexanoate (Sulfo-LC-SPDP) was  
271 purchased from ProteoChem (catalogue #c1118). Illustra NAP-25 columns (catalogue #17-0852-  
272 01) were purchased from GE Healthcare. All other chemicals and reagents were from standard  
273 commercial sources. N9 cells were cultured in Dulbecco's Modified Eagle Medium (with high  
274 glucose, L-glutamine, sodium pyruvate) supplemented with 10% fetal bovine serum (FBS),  
275 HEPES (0.01M), penicillin (100 U/mL), and streptomycin (100 µg/mL) incubated at 37°C in a  
276 humidified 5% CO<sub>2</sub> atmosphere. For movement experiments, cells were cultured in glassbottom  
277 dishes (MatTek Corporation, catalogue # P35G-0-14-C). Coverslip removal fluid (catalogue # P  
278 DCF OS 30) was obtained from MatTek.

#### 279 3.1. SPION-CpG synthesis

280 Silane-PEG-NH<sub>2</sub> (29 eq, 17mM) and Sulfo-LC-SPDP (17 eq, 10mM) were dissolved in  
281 deionized water and stirred for 2 hours at room temperature. Meanwhile, RSS-CpG (1 eq) was  
282 dissolved in deionized water containing at least 2.5mM DTT and stirred for 2 hours at room  
283 temperature. DTT-treated RSS-CpG was then passed through a nap-25 column (GE Healthcare)

284 in order to remove excess DTT. The CpG solution was then added to the Silane-PEG-NH<sub>2</sub>-  
285 containing reaction and heated in a 60 °C oil bath for at least 2 hours. After 2 hours, the reaction  
286 was isopropanol-precipitated, dialyzed against deionized water using a <3.5kD MWCO  
287 membrane, and lyophilized.

288 The lyophilized material was dissolved in deionized water and diluted to an effective  
289 CpG concentration of 2 mg/mL based on UV absorbance at 260 nm (RSSCpG  $\epsilon_{260\text{nm}} = 261900 \text{ L}$   
290  $\text{mol}^{-1} \text{ cm}^{-1}$ ). Then SPIONs (25 mg/mL in chloroform) were combined with the product stock  
291 solution in a 1:1 mass ratio (SPION : CpG). The mixture was rotated for 10 minutes and  
292 distributed into 1.5 mL microcentrifuge tubes with <1 mL in each. To disperse the SPIONs, the  
293 sample tubes were ultrasonicated for a process time of 4 h (80 amplitude, 15 s on, 15 s off). The  
294 SPION-CpG conjugates were then dialyzed (100 kD MWCO) against deionized water. After  
295 dialysis, the samples were diluted to a final concentration of 1 mg/mL SPIONs and 1 mg/mL  
296 RSSCpG (assuming no loss) using deionized water. During synthesis of SPION-CpG,  
297 discoloration of sample tubes and sedimentation upon dialysis membranes was observed,  
298 indicating that some of the material was lost. However, it was not feasible to quantify the SPION  
299 loss on these surfaces. Similarly, the amount of CpG lost during SPION-CpG synthesis is also  
300 difficult to quantify. Therefore as an approximation, the concentrations reported in subsequent  
301 experiments assumed no loss of SPIONs and no loss of CpG. At worst, when using this  
302 approximation we underestimated the immunostimulatory potential and cell uptake efficiency of  
303 SPION-CpG.

### 304 **3.2. Mass Spectrometry**

305 Using 3kD MWCO centrifugal spin filters (Amicon Ultra 0.5 mL, catalogue # UFC500324,  
306 EMD Millipore), crude from the RSSCpG reduction reaction was washed with an ammonium

307 acetate – acetic acid buffer (pH = 4.5) and deionized water for desalting. The sample was  
308 introduced by nanoelectrospray into a Thermo LTQ-FT operated in negative ion mode under  
309 manual control. Ions were detected in the ICR cell at resolution 100,000 (at m/z 400).

### 310 **3.3. NF $\kappa$ B activity assay**

311 RAW-Blue<sup>TM</sup> mouse macrophage reporter cells (Invivogen) were cultured at 5000 cells per well  
312 (using a 96-well plate; 6 repeat per group). Cells were treated with 10  $\mu$ L of RSSCpG, SPION-  
313 CpG, or water for 16 hours. Both RSSCpG and SPION-CpG treated wells had the same final  
314 CpG concentration (0.1 mg/mL). The level of secreted embryonic alkaline phosphatase (SEAP)  
315 was quantified by incubating 10  $\mu$ L of supernatant with 190  $\mu$ L QuantiBlue<sup>TM</sup> substrate  
316 (InvivoGen) for 1h and reading absorption at 620 nm using DTX 880 Multimode Detector  
317 (Beckman Coulter). QuantiBlue<sup>TM</sup> substrate was prepared by mixing one pouch of QUANTI-  
318 Blue in 100 mL of deionized water. The solution was then filtered using a 0.2  $\mu$ m membrane.  
319 QuantiBlue<sup>TM</sup> substrate was warmed at 37°C prior to use.

### 320 **3.4. Physical characterizations**

321 Dynamic light scattering (DLS) and zeta potential (ZP) measurements were performed (ionic  
322 strength  $10^{-3}$ M using NaCl) on a Brookhaven 90 Plus/Bi-MAS Instrument (Brookhaven  
323 Instruments, New York). DLS measurements were obtained by performing 10 runs at 30 s per  
324 run and the ZP values by measuring 10 runs involving 20 cycles per run. For the zeta potential  
325 measurements the samples were diluted to achieve an effective concentration of 0.01 w/v%  
326 (assuming no SPION loss). Each time, prior to performing DLS and ZP measurements the  
327 sample was ultrasonicated for 1 h.

### 328 **3.5. LIVE/DEAD staining and light microscopy**

329 Cytotoxicity assessment was performed using the LIVE/DEAD staining assay (Invitrogen). N9  
330 microglia cells seeded at  $9.6 \times 10^4$  cells per well in a glass bottom cell culture dish were grown to  
331 80% confluence. For each viability assay, the cells were washed with PBS, treated with the  
332 SPION-CpG conjugates and incubated for 12 h. After exposure to the different SPIONs, the cells  
333 were rinsed with PBS and stained with calcein-AM and ethidium homodimer (EthD-1 or EthD-  
334 2). The dyes were mixed together and appropriately diluted so that the effective working solution  
335 contains 2  $\mu\text{M}$  of calcein-AM and 4  $\mu\text{M}$  of ethidium homodimer which was then directly added  
336 to cells following manufacturer's protocol. After incubation with the dye, the cells were treated  
337 with fixative (either glutaraldehyde for post-movement SEM samples or paraformaldehyde) and  
338 imaged.

339 Light microscopy images were obtained on several instruments: Nikon Eclipse TS100  
340 microscope equipped with Infinity2 camera (Nikon Instruments Inc., USA), Nikon Eclipse  
341 TE2000-U Inverted Fluorescence microscope (Nikon Instruments Inc., USA), Zeiss Axio  
342 Observer Z1 Inverted microscope with a Hamamatsu EMCCD C9100-13 Monochrome Camera,  
343 and a Zeiss LSM 710 confocal laser-scanning microscope with a Plan-Apochromat  $20\times/0.8$   
344 objective (Carl Zeiss Microimaging, Thornwood, NY). For confocal images, optical sections  
345 were collected at 1  $\mu\text{m}$  spacing and shown as a maximum intensity projection using Zen 2009  
346 software (Carl Zeiss). For the Zeiss Axio Observer, Zen 2012 blue software was used.

### 347 **3.6. Inductively coupled plasma mass spectroscopy (ICP-MS) for uptake and exocytosis**

348 To quantify the total uptake of the SPION-CpG by the microglia N9 cells we performed ICP-MS  
349 (4500 Series, Hewlett Packard) measurements. The cells were grown as described above and  
350 treated with various concentrations of SPION-CpG (0, 0.01, 0.1, 0.3 and 0.5 mg/mL) or  
351 Ferumoxylol (1.5 mg/mL). After 12 h of exposure, the medium was aspirated, the cells were

352 washed once with PBS and were collected by treating with 0.2% trypsin-EDTA, followed by  
353 washing two times with PBS and table-top centrifugation (1000 rpm, 5 min), acid digested  
354 overnight using 1 mL of 67-70% BDH Aristar® Plus Nitric Acid, and analyzed using ICP-MS  
355 upon appropriate dilution. A standard curve was made using serial dilution of a 1ppm solution of  
356 Iron standard solution (Spex CertiPrep). Iron concentration was determined by ICPMS Analysis  
357 on a HP 4500 Series using a concentric nebulizer, Scott type spray chamber, and a fixed quartz  
358 injector torch. A CX interface was used. Plasma power was 1500 Watt. Helium was used as the  
359 collision gas (4 mL/min). Data was analyzed quantitatively in a spreadsheet program.

360 To evaluate exocytosis, N9 cells were plated at 6,000 cells per well in a 96 well plate  
361 ( $18,000 \text{ cells/cm}^2$ ) and allowed to adhere for 24 h. The cells were then loaded at a 0.1 mg/mL  
362 concentration of SPION-CpG for 2 h. After loading, the cells were washed twice with PBS and  
363 150  $\mu\text{L}$  fresh media was added to each well. At  $t = 0 \text{ h}$ , 8 h, and 24 h, media in the well was  
364 completely removed (“supernatant” fraction) and both the amount of iron in both the supernatant  
365 and cell fractions was quantified via ICP-MS. Each group was in triplicate and two independent  
366 experiments were performed.

367 ICP-MS for the exocytosis experiment was performed as follows: 200  $\mu\text{L}$  BDH Aristar  
368® Plus Nitric Acid (70%) was added to each sample tube (for the supernatant fraction) or well of  
369 a 96 well plate (cell fraction) to dissolve the iron. Each tube or well was washed once with 200  
370  $\mu\text{L}$  of 70% Nitric acid, the sample was then diluted to 3.4 mL with 3 mL of 2% nitric acid  
371 solution. Iron concentration was determined by ICPMS Analysis on Agilent 7500 Series using a  
372 concentric nebulizer, Scott type spray chamber, and a fixed quartz injector torch. A CX interface  
373 was used. Plasma power was 1500 Watt. Helium was used as the collision gas (4 mL/min). A

374 standard curve was made using serial dilution of a 1ppm solution of Iron standard solution (Spex  
375 CertiPrep). Data was analyzed quantitatively in a spreadsheet program.

### 376 **3.7. Dark-field microscopy imaging**

377 Cells were grown to 80% confluence on a glass bottom cell culture dish for 24-48 h. The cells  
378 were loaded with 0.5 mg/mL SPION-CpG for 2 h. After loading, excess media was removed,  
379 and the cells were washed extensively with PBS. The cover slips were carefully detached from  
380 the bottom of the dishes using a sharp edge forcep and allowed to dry. A drop of non-drying  
381 immersion oil (Cargille Laboratories, Cedar Grove, NJ) was put on the cover slip and the cover  
382 slip was mounted onto the glass slide and was adhered using nail polish to prevent drying. Dark-  
383 field microscopy imaging was performed using a CytoViva dark field microscope system  
384 equipped with CytoViva Hyperspectral Imaging System 1.2.

### 385 **3.8. Electron Microscopy (SEM and TEM)**

386 TEM imaging was performed on a FEI Tecnai 12 TEM equipped with a Gatan Ultrascan 2K  
387 CCD camera at an accelerating voltage of 120 kV. Cells treated with SPION-CpG conjugates  
388 (0.5 mg/mL) as described earlier, were collected by treating with 0.2% trypsin-EDTA, followed  
389 by washing with PBS and table top centrifugation (2000 rpm, 5 min), fixed with 2%  
390 glutaraldehyde in 0.1 M Cacodylate buffer ( $\text{Na}(\text{CH}_3)_2\text{AsO}_2 \cdot 3\text{H}_2\text{O}$ ), pH 7.2, at 4°C overnight.  
391 The following day the cells were washed three times with 0.1 M Cacodylate buffer, post-fixed  
392 with 1%  $\text{OsO}_4$  in 0.1 M Cacodylate buffer for 30 min and washed three times with 0.1 M  
393 Cacodylate buffer. The samples were then dehydrated using 60%, 70%, 80%, 95% ethanol and  
394 100% absolute ethanol (twice), propylene oxide (twice), and were left in propylene  
395 oxide/Eponate (1:1) overnight at room temperature under sealed environment. The following day  
396 the vials were left open until the propylene oxide was evaporated (~2-3 h). The samples were

397 infiltrated with 100% Eponate and polymerized at  $\sim 64^{\circ}\text{C}$  for 48 hours. Ultra-thin sections ( $\sim 70$   
398 nm thick) were cut using a Leica Ultra cut UCT ultra-microtome equipped with a diamond knife,  
399 and the sections were picked up on 200 mesh copper EM grids. The grids were stained with 2%  
400 uranyl acetate for 10 minutes followed by Reynold's lead citrate staining for a minute prior to  
401 imaging.

402 SEM images of the magnetically-moved cells were obtained on an FEI Quanta 200  
403 scanning electron microscope. Immediately after LIVE/DEAD staining, cells were fixed with 2%  
404 glutaraldehyde in 0.1M Cacodylate buffer ( $\text{Na}(\text{CH}_3)_2\text{AsO}_2 \cdot 3\text{H}_2\text{O}$ ), pH 7.2, at  $4^{\circ}\text{C}$ . The coverlip  
405 was then removed from the glassbottom dish using Coverslip Removal Fluid (MatTek) following  
406 the manufacturer's protocol. The coverslip was then washed three times with 0.1M Cacodylate  
407 buffer, pH 7.2, post-fixed with 1%  $\text{OsO}_4$  in 0.1M Cacodylate buffer for 30 min and washed three  
408 times with 0.1M Cacodylate buffer. The samples were then dehydrated through 60%, 70%, 80%,  
409 95% ethanol, 100% absolute ethanol (twice). The samples were dried in a critical-point dryer and  
410 then coated with gold and palladium (Au: Pd 60/40 ratio) in a Cressington 308R coating system.

### 411 **3.9. Magnetic-field induced qualitative cell movement *in vitro* by bright-field microscopy**

412 For the magnetically induced cell movement experiments, microglia N9 cells were cultured as  
413 described above. Cells were seeded at  $9.3 \times 10^5$  cells per dish ( $9.7 \times 10^4$  cells/cm<sup>2</sup>), grown to 90%  
414 confluence and treated with various concentrations (low; 0.1 mg/mL, medium; 0.3 mg/mL and  
415 high; 0.5 mg/mL) of SPION-CpG conjugates. After 2 h of incubation, the loading medium was  
416 aspirated, the cells were washed extensively with PBS (carefully, until most of the free SPION-  
417 CpG was gone), supplemented with fresh growth medium and were placed in the incubator with  
418 magnet placed underneath the dish separately. Further to show the controlled movement of cells,  
419 three different shapes of magnets were used; square, circular, and rectangular. The movement of

420 cells towards the magnet was assessed at various times (0 h, 2 h, 4 h and 20 h) using microscopy.  
421 In order to verify that increased iron concentration at the edge of the magnet was SPION-CpG-  
422 loaded cells and not free particles in solution, a cell-free SPION-CpG-only control was included.  
423 After movement, the cells were stained for iron using Prussian blue staining as per  
424 manufacturer's (Polyscience Inc. Warrington, PA) instructions. Briefly, equal volumes of 4%  
425 potassium ferrocyanide and 4% hydrochloric acid were mixed together to prepare the working  
426 solution. The standard staining required at least two changes of the working solution treatments  
427 for 10 minutes each. After which the cells were rinsed three times with distilled water and  
428 stained using nuclear fast red for 3 min. Finally, the cells are rinsed in running tap water for 1  
429 minute and imaged immediately.

### 430 **3.10. Cell box design**

431 An imaging apparatus was required to image, incubate, and magnetically manipulate cells loaded  
432 with SPION-CpG. The apparatus, or cell box, was inserted onto a petri dish containing cell  
433 media. It was comprised of a 3D printed ABS substrate (Fig S4Q) attached to a large coverslip  
434 (48 mm x 65 mm no 1, Ted Pella, catalogue #260365). The cell box provides an enclosed  
435 environment for long term cell viability and proliferation while allowing for external  
436 manipulation of magnet fields. In order to maintain the pH of cell media, exogenous CO<sub>2</sub> was  
437 supplied through the inlet port of the custom cell box and evenly distributed to distribution  
438 channels inside the petri dish. A pressure relief port prevented the accumulation of pressure and  
439 ensured a continuous flow of atmosphere.

440 The cell box was printed using a 3D printer (Replicator 2, Makerbot) and is both airtight  
441 and waterproof. The cell box features a hollow center to enable light illumination during bright

442 field microscopy. A slotted coverslip face allows for structural support of the coverslip and  
443 coverslip adhesive. The cell box was printed with ABS filament (ABS filament, Makerbot).

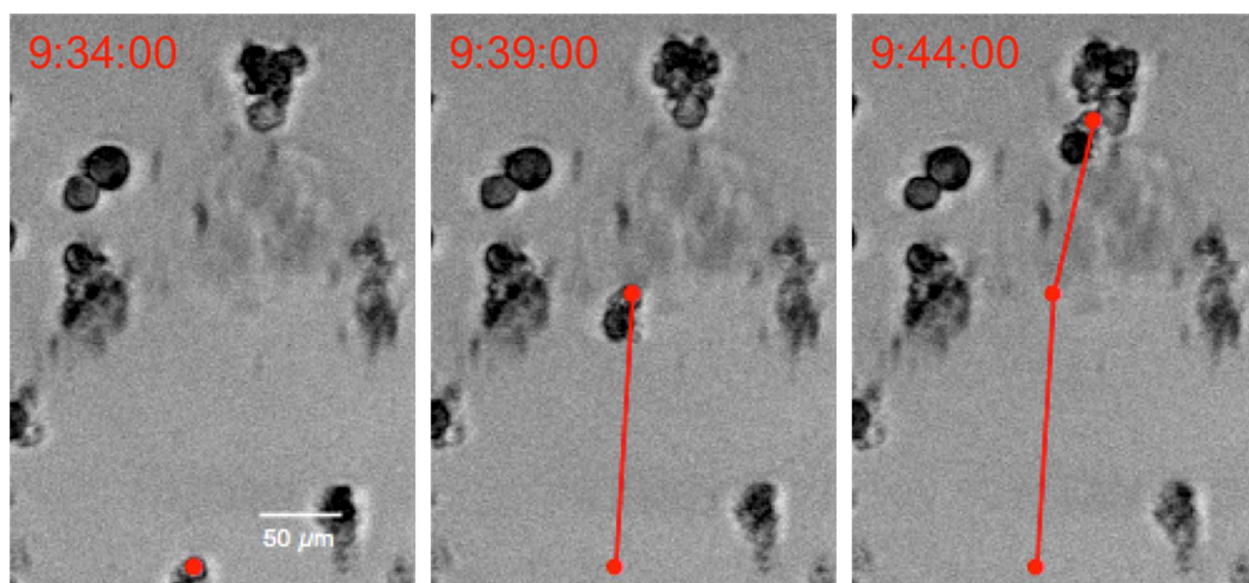
### 444 **3.11. Live cell imaging**

445 In preparation for live cell imaging, the cell box was assembled and N9 cells plated on it. The  
446 box was first sterilized by soaking in 0.6% NaOCl and rinsed thoroughly with autoclaved  
447 deionized water in order to remove residual NaOCl (bleach). A large coverslip (48 mm x 65 mm  
448 no 1, Ted Pella, catalogue #260365) was autoclaved and attached to the cell box using a non-  
449 cytotoxic silicone based adhesive (Silbione Med Adhesive 4100 RTV, Factor II, catalogue #A-  
450 4100). The box-coverslip assembly was then left at room temperature in a sterile environment  
451 (biosafety hood) for about 2 days in order to allow the adhesive to cure. After 2 days, an  
452 autoclaved polydimethylsiloxane (PDMS) dam was placed on the coverslip in order to form a  
453 makeshift tissue culture dish. The PDMS dam was created by first synthesizing a ~0.5 cm thick  
454 rectangular slab of PDMS on a clean glass surface (Sylgard 184 Silicone elastomer kit, Dow  
455 Corning, follow manufacturer's protocol) and then cutting an ~9 cm<sup>2</sup> rectangular hole in the  
456 PDMS. When this PDMS dam is set on the box-coverslip assembly, it forms a water-tight seal  
457 with the coverslip. Once the dam is in place, N9 cells ( $8.72 \times 10^5$  cells or  $9.7 \times 10^4$  cells/cm<sup>2</sup>) were  
458 plated on the coverslip and allowed to adhere for 8 h in the incubator. The cells were then loaded  
459 at 0.1 mg/mL SPION-CpG for 2 h, following the protocol for the previous cell movement  
460 experiment. After loading, the cells were washed with PBS, the PDMS dam was removed and  
461 the box-coverslip assembly was inverted into a 100 mm petri dish containing enough media to  
462 submerge the coverslip (10 – 20 mL).

463 Live cell imaging was performed on a Zeiss Axio Observer Z1 Inverted microscope with  
464 the Pecon/Zeiss Incubation System. Images were obtained using a 10x/ 0.3NA EC-Plan Neofluar

465 objective and a Hamamatsu EMCCD C9100-13 Monochrome Camera. The microscope and  
466 camera were controlled using the Zen 2012 Blue Edition software. After connecting the cell box  
467 to the microscope, pre-magnet images were taken for reference. A ceramic magnet was then  
468 placed on top of the coverslip portion of the cell box above the region of the coverslip where  
469 cells are adhered. To prevent the magnet from moving during the experiment, the magnet was  
470 secured to the coverslip with tape. Using time-lapse imaging (1 brightfield image every 30 s), the  
471 motion of cells within one field of view near the magnet were tracked over 20 h (the same time  
472 scale used for the other movement experiment).

473



474

475 **Figure 5:** Tracking magnetized cells under the exposure of a magnetic field. The cell position  
476 was calculated by identifying its centroid position.<sup>32</sup> The cell speed was calculated using the total  
477 distance traveled between consecutive frames.

478

### 479 3.12. Cell tracking

480 Magnetized cells were imaged inside the cell box for 20 h at a frame rate of 2 frames/min in  
481 order to observe long-term motility. The centroid position of the cell was determined using a  
482 computer vision algorithm as seen in Fig 5.<sup>32</sup> A 2D cross correlation was computed to determine  
483 position offsets in consecutive frames. All cells move in the same plane. The velocities of the  
484 cells were examined both in the direction of the magnet (positive vertical direction) as well as the  
485 horizontal direction, as seen in Fig 4A-B. The velocity of the cell from one frame to the next was  
486 calculated by multiplying the displacement in one frame by the frame rate.

487

#### 488 **4. Conclusions**

489 SPION-CpG conjugates were non-toxic to N9 microglia cells and were efficiently internalized  
490 into endosomal compartments. This enabled magnetic control over microglia motility *in vitro*.  
491 This work establishes the possibility of using a nanoparticle to both stimulate immune cells and  
492 to control their trafficking. Future experiments will investigate the optimal coating for the  
493 SPIONs to further enhance immune cell activation.

494

#### 495 **Acknowledgements**

496 We gratefully acknowledge ICP-MS instrumentation under the supervision of Nathan Dalleska at  
497 the Environmental Analysis Center at the California Institute of Technology. We thank Denise  
498 Keen from the Mass Spectrometry and Proteomics Core Facility at the Beckman Research  
499 Institute of the City of Hope for assistance with mass spectrometry. The authors gratefully  
500 acknowledge Marcia M. Miller, Zhuo Li and Ricardo Zerda for assistance with the TEM from

501 the COH Electron Microscope Core Facility. The authors gratefully acknowledge Brian  
502 Armstrong and Tina Patel for assistance with fluorescent and bright field microscopy from the  
503 Light Microscopy Digital Imaging Core. The authors gratefully acknowledge Kaushik Dasgupta  
504 and Jeff Sherman for their dedicated assistance in magnetic manipulation of magnetized cells.  
505 The authors would like to also thank Brian Hong for proofreading this manuscript. Finally, the  
506 authors would like to thank ONR N00014-02-1 0958 for funding for the TEM, NSF DBI-  
507 9970143 for funding for the Ultramicrotome, R21NS081594, R01CA155769, R21CA189223,  
508 City of Hope-Caltech Biomedical Research Initiative, The Kenneth T. and Eileen L. Norris  
509 Foundation, STOP Cancer, and the ThinkCure! Foundation for research funding. Research  
510 reported in this publication included work performed in the Light Microscopy Digital Imaging  
511 and Electron Microscopy Cores supported by the National Cancer Institute of the National  
512 Institutes of Health under award number P30CA33572.

513

514 **Electronic Supplementary Material:** Supplementary material with the transmission electron  
515 microscopy images of the particles, additional independent experiments for the NF $\kappa$ B activity  
516 and exocytosis assays, TEM images for the SPION untreated cells, bright field microscopy  
517 images of the cells alone in the presence and absence of magnet, images of the magnetic  
518 movement experiments at higher doses of SPION, full uncropped images of the post-migration  
519 LIVE/DEAD assay, and a video file of cell movement is available in the online version of this  
520 article.

## 521 **References**

522 1. I. Mellman, G. Coukos and G. Dranoff, *Nature*, 2011, **480**, 480-489.

- 523 2. Y. Meng, M. Kujas, Y. Marie, S. Paris, J. Thillet, J. Y. Delattre and A. F. Carpentier, *J Neurooncol*,  
524 2008, **88**, 19-25.
- 525 3. S. F. Hussain, D. Yang, D. Suki, E. Grimm and A. B. Heimberger, *J Transl Med*, 2006, **4**, 15.
- 526 4. S. F. Hussain, D. Yang, D. Suki, K. Aldape, E. Grimm and A. B. Heimberger, *Neuro Oncol*, 2006, **8**,  
527 261-279.
- 528 5. M. Bsibsi, R. Ravid, D. Gveric and J. M. van Noort, *Journal of neuropathology and experimental*  
529 *neurology*, 2002, **61**, 1013-1021.
- 530 6. E. Latz, A. Schoenemeyer, A. Visintin, K. A. Fitzgerald, B. G. Monks, C. F. Knetter, E. Lien, N. J.  
531 Nilsen, T. Espevik and D. T. Golenbock, *Nature immunology*, 2004, **5**, 190-198.
- 532 7. B. Badie and J. M. Berlin, *Immunotherapy*, 2013, **5**, 1-3.
- 533 8. M. A. Dobrovolskaia, P. Aggarwal, J. B. Hall and S. E. McNeil, *Molecular pharmaceuticals*, 2008, **5**,  
534 487-495.
- 535 9. Y. Suzuki, D. Wakita, K. Chamoto, Y. Narita, T. Tsuji, T. Takeshima, H. Gyobu, Y. Kawarada, S.  
536 Kondo, S. Akira, H. Katoh, H. Ikeda and T. Nishimura, *Cancer Research*, 2004, **64**, 8754-8760.
- 537 10. S. Rattanakit, M. Nishikawa and Y. Takakura, *Eur J Pharm Sci*, 2012, **47**, 352-358.
- 538 11. S. L. Demento, N. Bonafe, W. G. Cui, S. M. Kaech, M. J. Caplan, E. Fikrig, M. Ledizet and T. M.  
539 Fahmy, *Journal of Immunology*, 2010, **185**, 2989-2997.
- 540 12. M. Wei, N. Chen, J. Li, M. Yin, L. Liang, Y. He, H. Y. Song, C. H. Fan and Q. Huang, *Angew Chem Int*  
541 *Edit*, 2012, **51**, 1202-1206.
- 542 13. D. C. Zhao, D. Alizadeh, L. Y. Zhang, W. Liu, O. Farrukh, E. Manuel, D. J. Diamond and B. Badie,  
543 *Clinical Cancer Research*, 2011, **17**, 771-782.
- 544 14. H. Fan, I. Zhang, X. Chen, L. Zhang, H. Wang, A. Da Fonseca, E. R. Manuel, D. J. Diamond, A.  
545 Raubitschek and B. Badie, *Clin Cancer Res*, 2012, **18**, 5628-5638.
- 546 15. S. C. McBain, H. H. Yiu and J. Dobson, *Int J Nanomedicine*, 2008, **3**, 169-180.
- 547 16. B. Shapiro, *Journal of magnetism and magnetic materials*, 2009, **321**, 1594.
- 548 17. A. Nacev, S. H. Kim, J. Rodriguez-Canales, M. A. Tangrea, B. Shapiro and M. R. Emmert-Buck,  
549 *International Journal of Nanomedicine*, 2011, **6**, 2907-2923.
- 550 18. B. Chertok, B. A. Moffat, A. E. David, F. Yu, C. Bergemann, B. D. Ross and V. C. Yang,  
551 *Biomaterials*, 2008, **29**, 487-496.
- 552 19. S. V. Pislaru, A. Harbuzariu, R. Gulati, T. Witt, N. P. Sandhu, R. D. Simari and G. S. Sandhu, *J Am*  
553 *Coll Cardiol*, 2006, **48**, 1839-1845.
- 554 20. B. Polyak, I. Fishbein, M. Chorny, I. Alferiev, D. Williams, B. Yellen, G. Friedman and R. J. Levy,  
555 *Proc. Natl. Acad. Sci. U. S. A.*, 2008, **105**, 698-703.
- 556 21. P. G. Kyrtatos, P. Lehtolainen, M. Junemann-Ramirez, A. Garcia-Prieto, A. N. Price, J. F. Martin, D.  
557 G. Gadian, Q. A. Pankhurst and M. F. Lythgoe, *JACC. Cardiovascular interventions*, 2009, **2**, 794-  
558 802.
- 559 22. A. S. Arbab, E. K. Jordan, L. B. Wilson, G. T. Yocum, B. K. Lewis and J. A. Frank, *Human gene*  
560 *therapy*, 2004, **15**, 351-360.
- 561 23. V. Vanecek, V. Zablotskii, S. Forostyak, J. Ruzicka, V. Herynek, M. Babic, P. Jendelova, S.  
562 Kubinova, A. Dejneka and E. Sykova, *Int J Nanomedicine*, 2012, **7**, 3719-3730.
- 563 24. A. Yanai, U. O. Hafeli, A. L. Metcalfe, P. Soema, L. Addo, C. Y. Gregory-Evans, K. Po, X. Shan, O. L.  
564 Moritz and K. Gregory-Evans, *Cell transplantation*, 2012, **21**, 1137-1148.
- 565 25. E. S. Jang, J. H. Shin, G. Ren, M. J. Park, K. Cheng, X. Chen, J. C. Wu, J. B. Sunwoo and Z. Cheng,  
566 *Biomaterials*, 2012, **33**, 5584-5592.
- 567 26. S. Laurent, D. Forge, M. Port, A. Roch, C. Robic, L. Vander Elst and R. N. Muller, *Chemical*  
568 *reviews*, 2008, **108**, 2064-2110.

- 569 27. Y. Sahoo, H. Pizem, T. Fried, D. Golodnitsky, L. Burstein, C. N. Sukenik and G. Markovich,  
570 *Langmuir*, 2001, **17**, 7907-7911.
- 571 28. T. Haas, J. Metzger, F. Schmitz, A. Heit, T. Müller, E. Latz and H. Wagner, *Immunity*, 2008, **28**,  
572 315-323.
- 573 29. R. T. Castaneda, A. Khurana, R. Khan and H. E. Daldrup-Link, *Journal of visualized experiments* :  
574 *JoVE*, 2011, e3482.
- 575 30. N. L. Rosi, D. A. Giljohann, C. S. Thaxton, A. K. Lytton-Jean, M. S. Han and C. A. Mirkin, *Science*,  
576 2006, **312**, 1027-1030.
- 577 31. P. C. Patel, D. A. Giljohann, W. L. Daniel, D. Zheng, A. E. Prigodich and C. A. Mirkin, *Bioconjugate*  
578 *chemistry*, 2010, **21**, 2250-2256.
- 579 32. T. L. Hedrick, *Bioinspiration & Biomimetics*, 2008, **3**, 034001.

580

581